HOPF BIFURCATION, LANDAU EQUATION, AND VORTEX SHEDDING BEHIND CIRCULAR CYLINDERS

K. R. Sreenivasan, P. J. Strykowski, and D. J. Olinger
Department of Mechanical Engineering and Center for Applied Mechanics
Yale University
New Haven, Connecticut

Abstract

We show by experiment that the bifurcation accompanying the vortex shedding behind circular cylinders is of the Hopf type, and that the Landau equation (with constants possibly depending on the spatial position) describes the post-critical behavior quite accurately. We determine typical Landau constants. Finally, we examine the sense in which absolute instability is relevant to the vortex shedding problem.

1. Introduction

It is well known that the flow behind circular cylinders is steady up to a certain critical Reynolds number. Beyond this critical value, the flow develops into a periodic state, corresponding to the formation behind the cylinder of two rows of staggered vortices of opposite sign - the so-called Karman vortex street. The downstream distance up to which this 'street' survives behind the cylinder depends on the Reynolds number.

There are three main points of interest here. First, we would like to establish by experiment the precise nature of the bifurcation occurring at the critical Reynolds number; we shall show that the bifurcation is strictly of the Hopf type. Landau (see, for example, Landau & Lifshitz 1959, p103) proposed a simple model equation to describe the post-critical state of a system undergoing supercritical bifurcation of the Hopf type. Our second objective is to make measurements specifically designed to answer the question of how well the Landau equation describes the post-critical state in the wake problem. Finally, we discuss the sense in which our measurements support the notion that the vortex shedding process in wakes is governed by absolute instability.

2. Hopf bifurcation

We consider the basic state of the system as being perturbed by a disturbance. First, we ignore all spatial dependence and consider only the temporal development; we shall later review why this seemingly inappropriate approximation is the right one for the wake. The disturbance decays in time to zero amplitude if the system is stable, or grows to reach a saturation amplitude if the basic system is unstable. The phase representation of this latter state is a limit cycle.

Let u_r and u_i be the real and imaginary parts of the perturbation velocity. If we plot u_i and u_r against the Reynolds number Re, all small perturbations below the critical Reynolds number Re_{cr} wind down to zero. Above Re_{cr}, all small perturbations grow exponentially with time, and eventually asymptote to a finite amplitude $u_{os} \sim (Re - Re_{cr})^{0.5}$. The situation is illustrated in figure 1a. Further, writing

$$[\dot{u}] = [A][u] , \qquad (2.1)$$

the dot denoting the time derivative, we require for Hopf bifurcation that the eigenvalues of the matrix A(Re) be complex conjugates of each other, $\lambda_r \pm i\lambda_i$, say, reside in the left half of the complex plane for $Re < Re_{cr}$, and cross the imaginary axis at Re_{cr}. We further require that the speed at which the eigenvalues cross the imaginary axis, $d\lambda_r/dRe$, be positive and finite (figure 1b). We shall determine by measurement if these conditions accompany the vortex shedding process.

(a)

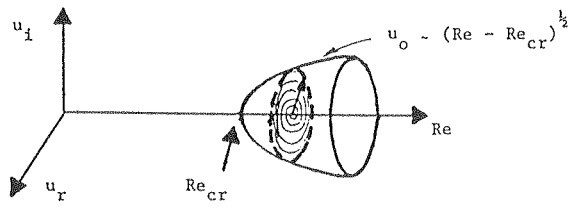

(b)

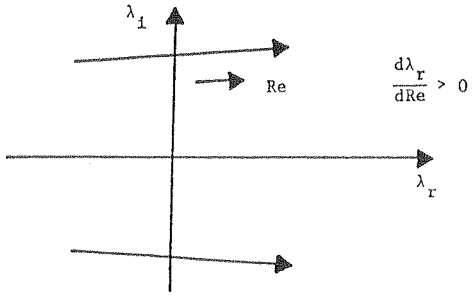

Figure 1 Hopf bifurcation

3. Experimental Facilities and Instrumentation

3.1 Wind Tunnels

All measurements made in the wake of the circular cylinder were performed in two pressure driven wind tunnels. The tunnels were supplied with compressed dry air from two large storage tanks. One of the tunnels was a carefully designed, low turbulence facility in which all spectral data (not shown here) were obtained. The second tunnel was designed especially for measuring temporal growth and decay rates in the wake, although the low-turbulence facility has also been used for the purpose.

3.1a Low turbulence facility: Air entered two settling chambers packed with damping material, downstream of which were two contractions with several carefully placed screens in between; see Strykowski (1986) for details. The settling chambers were acoustically lined with convoluted foam, and the upstream and downstream contractions had area ratios of 9:1 and 6:1 respectively. The whole arrangement produced, in the empty tunnel, a turbulence level $u'/U_o < 0.04\%$ over the entire range of velocities investigated; u' here is the root-mean-square (*rms*) magnitude of the streamwise velocity whose mean is U_o. The *rms* turbulence levels were measured from hot wire signals filtered from DC to 5 kHz and integrated over long time intervals (typically one minute). Downstream of the second contraction was located a test chamber of circular cross section. The test section was 5 cm in diameter and 10 cm long; it was carefully diverged to produce constant velocity throughout. The flow velocity U_o entering the test section from the second contraction was uniform across the test section to within 1% (outside the wall boundary layers).

3.1b Tunnel designed to measure amplification and decay rates: A second wind tunnel was employed to measure temporal growth and decay rates in the wake. The tunnel provided a steady mean flow but was designed with only a single contraction and could not be considered a good 'low turbulence' tunnel. Upstream of a large settling chamber were placed large needle and globe valves. The needle valve was used to adjust the speed and the globe valve enabled the flow to be rapidly set into motion or brought to rest; this will be required for the experiments to be described later. To enhance the response of the system, oversized pipes were used to connect the settling chamber to the two storage tanks (combined storage volume of approximately 18 m^3 at a storage pressure of 8×10^5 N/m^2).

Well polished drill rods, tensioned across the test section, were fitted with end plates to allow variation in aspect ratio and to provide better end conditions. The plates were designed following Stansby (1974); detailed measurements were made at aspect ratios, L/D, of 60, 27 and 14. A summary of the relevant diameters, aspect and blockage ratios is given in Table 1.

Table 1

Nomenclature:

D ... Cylinder diameter.
L ... Cylinder length between end plates.
H ... Height of test section normal to cylinder axis and freestream.

Low Turbulence Wind Tunnel

D (cm)	L/D	H/D
0.083	60.0	60.0

Single Contraction Wind Tunnel

D (cm)	L/D	H/D
0.147	60.0	72.0
0.147	27.0	72.0
0.147	14.0	72.0
0.318	60.0	33.0
0.183	60.0	55.0

3.2 Instrumentation

Some of the results to follow were obtained with DANTEC constant temperature hot wire anemometers, type 55M01, using 5μm wires etched to a working length of approximately 0.8mm; overheat ratios of 1.75 were used. The resulting data were DC offset and filtered with a DANTEC signal conditioner, model 55D26, and amplified to optimize the 12-bit resolution (±5 Volts) of the MASSCOMP MC-500 series computer. All data processing was done on this machine. During the initial stages of the work, it was felt that the hot wire probe, when placed within a few diameters of the cylinder, might be intruding with some details of flow development. Thus, all hot wire measurements were made outside of this sensitive region. Within this region, velocity measurements were made with a TSI laser Doppler velocimeter used in the forward scatter mode. In many instances where both LDV and hot wire were deemed reliable, both were used under identical circumstances as a check on each other.

Mean velocity was generally obtained using a Pitot-tube and a MKS-Baratron unit with a 10 Torr differential pressure head. At very low velocities (corresponding to Re < 20) the speed was determined by measuring the shedding frequency from several larger cylinders placed in the test section (in all cases the aspect ratios of the cylinders were never less than approximately 50). The velocity was then deduced from Roshko's (1955) expression relating frequency of shedding behind these larger cylinders and their Reynolds number:

$$fD^2/\nu = 0.212\,Re - 4.5. \qquad (3.1)$$

4. Experimental results

4.1 Temporal growth rates

Let us first concentrate on growth rates. The experiments needed to determine them must ideally consist of abruptly setting up the flow at a desired Reynolds number above the critical value, and observing how the oscillations grow in time. If the growth rate is exponential, one can obtain a_r from the expectation that initially the amplitude u_o grows exponentially:

$$u_o \sim \exp(a_r t) \qquad (4.1)$$

The procedure we adopted for determining growth rates was the following. The globe valve mentioned in section 3.1b was opened suddenly, and the streamwise velocity signal at the chosen location within the wake was digitally recorded. To avoid unnecessary changes in the mass flow rate, and to improve the effective time constant for the rise time of the mean velocity, the flow rate was increased from a value slightly below Re_{cr} (where no fluctuations exist) to the desired Reynolds number above Re_{cr} at which the oscillations begin to grow.

A typical oscillogram of velocity fluctuations is given in figure 2. The top trace, figure 2(a), corresponds to the mean velocity rise in the flow, measured slightly upstream of the cylinder. The accompanying flow Reynolds number variation is from 43 to 49, occurring in a time scale of the order of 200 msec which, as we shall see, is sufficiently small compared with the growth period of the velocity fluctuations. In fact, this characteristic rise time attainable for the mean velocity will limit the largest growth rate we can measure in our experiments. The bottom trace, figure 2(b), shows the manner in which the oscillations at x/D = 10 grow with time. The signal in figure 2(a) was low pass filtered below 30 Hz so as to reflect only the mean velocity variations, while the trace in figure 2(b) was high pass filtered above 30 Hz to eliminate the mean velocity variation. The shedding frequency was substantially larger than 30 Hz so that this high pass filtering does not introduce any artificial phase or frequency modifications in the oscillations. The traces in figure 2 were recorded

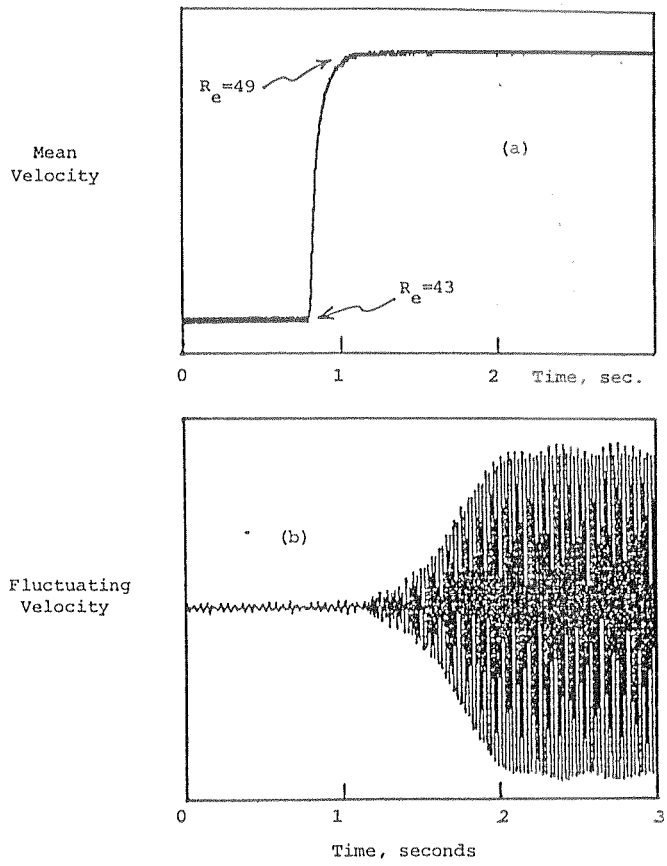

Figure 2: Simultaneous records of the mean and fluctuating velocities. The flow Reynolds number, R_e, was increased from 43 to 49. Trace (a) was low pass filtered below 30 Hz and trace (b) was high pass filtered above 30 Hz.

simultaneously and indicate that the oscillations commence only after the Reynolds number attains the supercritical state; hence, it is clear that the characteristics of the oscillations correspond unambiguously to this Reynolds number. The mean and the fluctuation responses were obtained by two different hot wires arranged in a non-intrusive way. The one used to obtain the mean flow response was placed slightly upstream of the cylinder, and so a time shift due to convection, of approximately 40 msec., must be made before a direct comparison of figures 2(a) and 2(b) is possible. The amplitude of the envelope in figure 2(b) can now be processed to obtain the growth rates. The logarithm of the amplitude envelope (figure 3a) plotted against time in figure 3(b) shows a linear region whose slope gives the constant a_r at the Reynolds number corresponding to the upper plateau in figure 2a.

Similar LDV measurements made at 5 diameters downstream of the cylinder show exactly the same features; the growth rates are not a function of position. It should be noted that as one gets closer to the cylinder than, say, 2.5 diameters, the growth rates are hard to measure, and some anomolies have been observed. We shall not discuss them here.

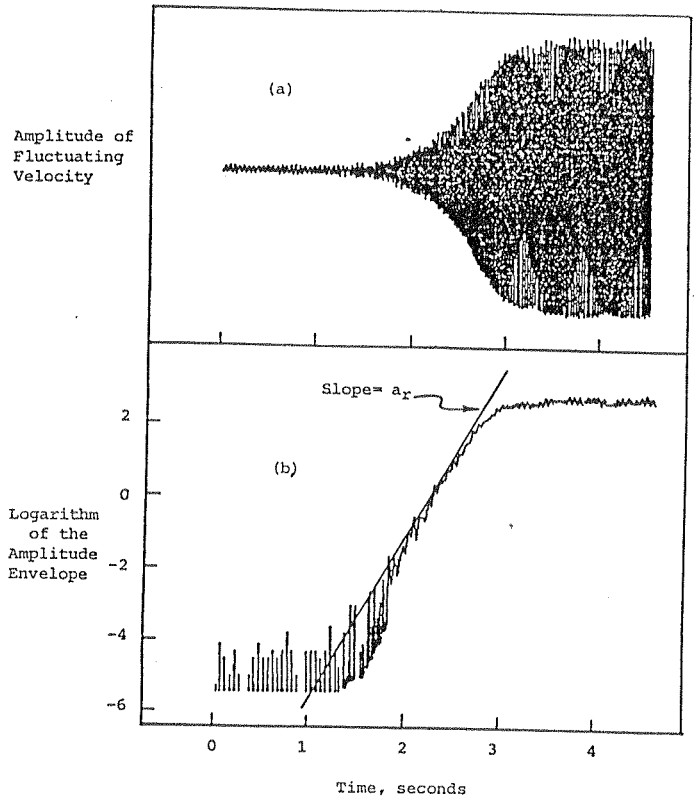

Figure 3: Trace (a) is the amplitude of the fluctuating velocity. The logarithm of the amplitude envelope is plotted in (b). The Reynolds number is 49 and a_r= 4.0 sec^{-1}.

4.2 Decay rates

While the measurement of growth rates as described above is in principle a relatively simple matter, the same cannot be said of the decay rates. In determining the growth rates, we set the flow instantly (in principle) to the required Reynolds number, and watch how the oscillations grow. Since the ground state here (being below Re_{cr}) does not possess any oscillations, the flow is free to choose the frequency and amplitudes appropriate to that Reynolds number. Since the natural state at Reynolds numbers below Re_{cr} is steady, it is clear that oscillations can be established only by means of some external forcing.The correct procedure in the decay measurements would therefore be to establish (by some external means) flow oscillation at the right frequency appropriate to any desired Reynolds number below Re_{cr} , and switch off the forcing to quantify the ensuing decay of the flow oscillation. One does not a priori know what the right forcing frequency should be, or how the decay rates depend on this frequency. Part of the work reported here concerns these questions.

Flow oscillations at the desired subcritical Reynolds number were set up in two different ways: (a) by mechanically oscillating the cylinder at the desired frequency, and (b) by acoustically exciting the oscillations in the flow behind the steady cylinder. In both cases, flow oscillations could be set up at any desired subcritical Reynolds number. The source of excitation was then switched off and the decay of oscillations in the wake was recorded either by a hot-wire (located at x/D >7) or the LDV. The decay rates of the wake oscillations were again observed to be exponential (see figure 4), and the coefficient a_r in equation (4.1) was obtained in a similar fashion to the growth case. The difference is that a_r is negative during decay.

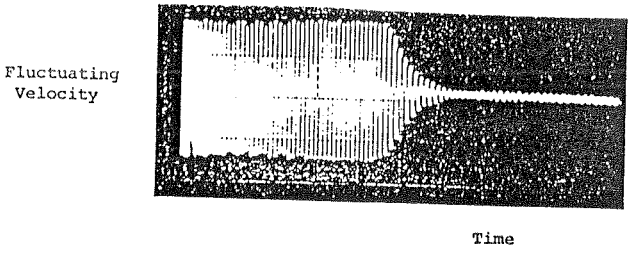

Figure 4: Mean and fluctuating velocity response, measured during decay. The flow Reynolds number is reduced from 50 to 44. Signal measured at x/D = 10 in shear layer.

We tried several excitation frequencies. Our first choice was the frequency with the least damping in the steady basic state for Re < Re_{cr}; from the work of Nishioka & Sato (1978) we know that large amplitude forcing at this special frequency can indeed set up vortex shedding even below Re_{cr}. Oscillations could be set up at other frequencies also, the point to note being that at these other freqencies the amount of external excitation required to produce sizeable flow oscillations is rather large. We have used as an example the frequency corresponding to a backward extrapolation of Roshko's relation (3.1). In this case too, the decay rates following the removal of the

cylinder excitation was exponential, with the same decay rates as before.

The measured growth and decay rates are collected in figure 5. Only one set of growth rate data has been plotted, but other sets obtained at different x/D, y/D, and by LDV as well as hot wires were no different except that the uncertainty in the data obtained at larger downstream distances was somewhat larger both because of the smaller amplitudes and possible three dimensional effects. It is clear that the exponent a_r varies linearly with the Reynolds number in a certain nontrivial neighborhood of Re_{cr}.

A remark seems useful on why we have normalized the growth

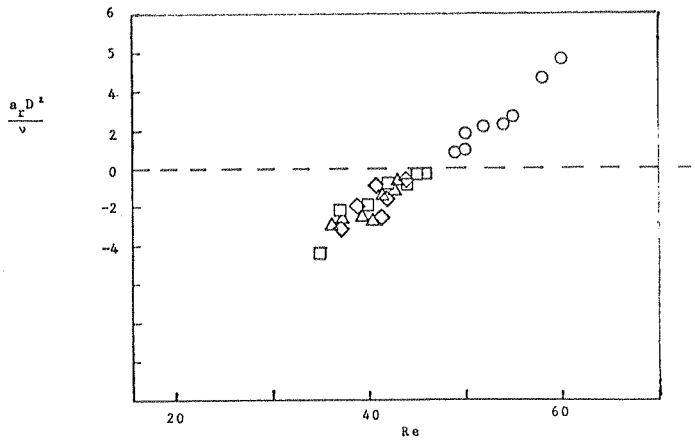

Figure 5: Growth and decay rates. ○ , turbulence level = 0.09%. □ , decay rates for acoustically excited oscillations; △ , decay of oscillations excited by cylinder oscillations, St = 0.1; ◇ , same as before, oscillation frequency given by Roshko's relation (3.1).

and decay rate data in figure 5 by the viscous time scale D^2/ν instead of the convective time scale D/U_o which, a priori, can be considered equally legitimate. The choice appears natural in view of the fact that $a_r D^2/\nu$ is usually of the order unity while $a_r D/U_o$, which is smaller by the factor of the Reynolds number, gives numerical values on the order 0.01.

The main conclusion then is that there exists a certain neighborhood of Re_{cr} in which the growth and decay rates behave according to

$$Re_{cr} = 46, \text{ and } d(a_r D^2/\nu)/dRe = 0.20. \qquad (4.2)$$

These numbers are independent of the measurement location, as well as (in the case of decay) of the excitation frequency. Both of them vary with the aspect ratio of the cylinder. Detailed growth rate measurements were made for aspect ratios of 60, 27 and 14 (figure 6). Obviously, the critical Reynolds number corresponding to zero growth rate is seen to be a function of the aspect ratio, as has been pointed out, for example, by Nishioka & Sato (1974). For the aspect ratios mentioned above, the critical Reynolds numbers were respectively 46, 50 and 53, in reasonable agreement with the data of

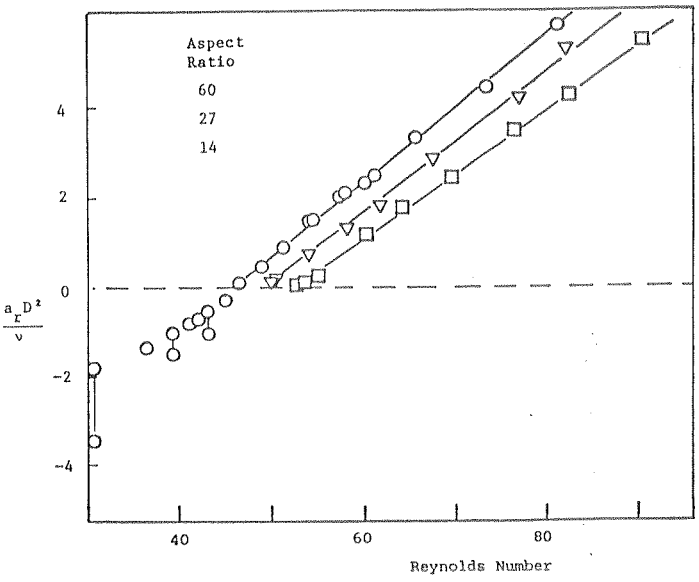

Figure 6: Amplification and decay rate measurements taken at an aspect ration of 60; amplification rates only for aspect rates of 27 and 14.

Nishioka & Sato. Less detailed measurements showed that the critical Reynolds number for the aspect ratio of 200 was also 46 in the present experiments, and therefore the results for the aspect ratio of 60 are believed to represent the essentials of the phenomena for an infinitely long cylinder. The decay rate measurements were restricted to the aspect ratio of 60.

The upper Reynolds number range for the growth rate measurements was set by the following two conditions. The first is that the higher the Reynolds number, the less adequate it is to assume that the mean velocity rise is essentially instantaneous on the scale of a_r^{-1}. Secondly, as was pointed out by Sreenivasan (1985) in another context, the periodic state at higher Reynolds number is modulated by higher order modes, and the measured exponential growth rates have a less satisfactory interpretation. The measurements presented here do not suffer from either of these two problems.

It is clear that the flow oscillations take a very long time to develop if one is in very close positive vicinity of Re_{cr}. It is truly exciting to watch vortex shedding appear just above Re_{cr}, say Re_{cr} + 1. The growth rates there are so small that saturation amplitudes are reached only for long times of the order of a minute corresponding to convective scales of the order 10^4; it is thus clear that vortex shedding at these Reynolds numbers is unrelated to any spatial development in the flow. In one case, we observed the growth phase extending for over one minute followed by an immediate decay over a comparable period of time; apparently, the Reynolds number had inadvertently fallen from just above to just below Re_{cr}.

4.3 The saturation amplitude

After the initial growth period, the amplitude saturates to a final value (see for example figure 2b). Here, we measure the maximum of

the amplitude of oscillation as a function of the flow Reynolds number at different locations in the wake. Figure 7 shows that this amplitude, squared, is a linear function of the Reynolds number. Again, the intercept on the Reynolds number axis gives us another estimate of the critical Reynolds number. Not surprisingly, this estimate agrees well with the previous one given by (4.2). This holds true for measurements at all locations in the wake. Saturation amplitudes have been made at a few streamwise locations in the flow, but the data are not detailed enough to decide whether or not the slope of the straight line in figure 7 is dependent on the spatial position in the wake. The available evidence, even though not sufficiently conclusive, suggests that the slope might in fact vary with x/D, although by not much in the region $3 < x/D < 7$.

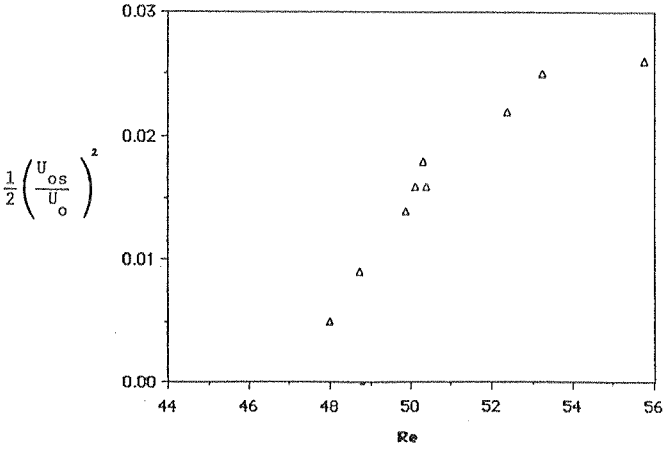

Figure 7: The saturation amplitude at x/D = 5, y/D = 0.5 in the wake of the cylinder.

2.5 The Periodic (Vortex Shedding) State and the Landau Equation

It will now be shown that the results of the previous section are consistent with the dictates of the Landau equation. We then deduce further consequences of the Landau equation, and examine them for consistency with measurements. The equation under question was formulated by Landau in the belief that it describes some universal features of an unstable system in some finite (but small) region in the vicinity of the critical Reynolds number (or some other control parameter relevant to the problem). In the present context, it can be written as

$$d\mathbf{u}/dt = \mathbf{a}\,\mathbf{u} - \mathbf{c}\,|\mathbf{u}^2|\,\mathbf{u} \qquad (5.1)$$

where **u** is the (complex) velocity fluctuation, and **a** and **c** are both (in general) complex constants. Writing $\mathbf{u} = u_o \exp[\, i\phi(t)\,]$ we have:

$$du_o/dt = a_r u_o - c_r u_o^3 \qquad (5.2)$$

governing the real part, and

$$d\phi/dt = a_i - c_i u_o^2 \qquad (5.3)$$

governing the imaginary part. Equation (5.1) can be solved exactly (see Landau and Lifshitz 1959), but our purposes are served adequately by noting the following features. Focusing first on equation (5.2), it is clear that all stable states are given by the condition $a_r < 0$ and c_r positive. As the basic state becomes unstable, a_r will change sign from negative to positive; the Reynolds number at which it happens will in fact define the critical Reynolds number Re_{cr}. In the linear regime, the second term on the right hand side is negligible, and the disturbance will grow in the usual exponential manner at a rate that depends on the magnitude of a_r. As the amplitude increases, nonlinear effects will become important, and the amplitude saturates to a certain level. The saturation state is given by the condition $du_o/dt = 0$ in (5.2), or

$$u_{os} = (\, a_r / c_r \,)^{0.5} \qquad (5.4)$$

where the suffix s denotes the saturation amplitude of u_o.

Following Landau, we may expand a_r in terms of the Reynolds number, and write a_r in a certain nontrivial neighborhood of Re_{cr} as:

$$a_r(Re) = a_r(Re_{cr}) + da_r/dRe\,(\,Re - Re_{cr}\,) + \ldots \qquad (5.5)$$

Clearly, $a_r(Re_{cr}) = 0$ by definition (see previous paragraph), and we have

$$a_r(Re) = da_r/dRe\,(\,Re - Re_{cr}\,). \qquad (5.6)$$

That is, the growth (or decay) rates are a linear function of the Reynolds number in the vicinity of Re_{cr} – as observed in the experiments (see figure 5).

Combining (5.6) with (5.4), we obtain the expression

$$u_{os}^2 = (1/c_r)\;da_r/dRe\,(\,Re - Re_{cr}\,). \qquad (5.7)$$

In general, c_r can also be expected to be a function of Reynolds number, and a Taylor series expansion can be made in the vicinity of Re_{cr}. Equation (5.7) then yields

$$u_{os}^2 = (1/c_{ro})\,da_r/dRe\,(Re - Re_{cr}) - \frac{da_r/dRe\,(Re - Re_{cr})2\;d_{cr}/dRe}{c_{ro}^2 + dc_r/dRe\;(Re - Re_{cr})c_{ro}} \qquad (5.8)$$

where $c_{ro} = c_r(Re_{cr})$. In general, if $(Re - Re_{cr})$ is small enough, the first term in (5.8) is an adequate representation of u_{os}^2, and we have

$$u_{os} = (1/c_{ro})^{1/2} (da_r/dRe)^{1/2} (Re - Re_{cr})^{1/2}, \qquad (5.9)$$

This states that the saturation amplitude increases as the half power of the difference Reynolds number ($Re - Re_{cr}$). We saw in section 4.3 that (5.9) is valid even if ($Re - Re_{cr}$) is not too small, implying that (dc_r/dRe) = 0 over a range of Reynolds numbers. Expressions (5.6) and (5.7) suggest that the constants da_r/dRe and c_{ro} can be determined if (a) the growth rates a_r and (b) the saturation amplitudes u_{os} can be measured as a function of the Reynolds number in the vicinity of Re_{cr}. This is precisely what we did in section 4. Note that da_r/dRe (=$0.2\nu/D^2$ for aspect ratios of the order 60 and above) is independent of position in the wake, but that, if our earlier statement on the slope of the line in figure 7 is correct, c_{ro} must be position-dependent. Our results at this point are not sufficiently complete to specify this dependence confidently, but it seems that c_{ro} does not vary all that strongly in the range $3 < x/D < 7$. So, the value quoted here ($c_{ro}D^2/\nu = 67$), as determined from figure 7 via (5.9) and (4.2), must tentatively be considered representative.

To determine the constants a_i and c_i, we have to turn to the imaginary part of the Landau equation. Noting that $d\phi/dt = 2\pi f$, where f is the frequency of oscillations in the disturbed state, we may write (5.3) as:

$$2\pi f = a_i - c_i u_o^2 \qquad (5.10)$$

In the saturated state, $u_o = u_{os}$ given by (10), and so we have after a little rearrangement:

$$fD^2/\nu = a_{io}D^2/2\pi\nu + (1/2\pi)\,[\, d(a_iD^2/\nu)/dRe - (c_{io}/c_{ro})\, d(a_rD^2/\nu)/dRe \,]\,(Re - Re_{cr}) - (1/2\pi c_{ro})\, d(a_rD^2/\nu)/dRe\, (Re - Re_{cr})^2\, dc_i/dRe, \qquad (5.11)$$

where again a_i and c_i have been expanded in terms of Re around Re_{cr}, and $a_{io} = a_i(Re_{cr})$, and $c_{io} = c_i(Re_{cr})$. The last term in equation (5.11) depends quadratically on the difference Reynolds number and can be neglected based on the well known empirical finding (equation 3.1) that the frequency in the saturation state varies linearly with ($Re - Re_{cr}$). Further substantiation that the quadratic term can be neglected will be provided later, where we show that $dc_i/dRe = 0$ over a range of ($Re - Re_{cr}$).

Dropping the nonlinear term from equation (5.11) we get,

$$fD^2/\nu = a_{io}D^2/2\pi\nu + (1/2\pi)[\, d(a_iD^2/\nu)/dRe - (c_{io}/c_{ro})\, d(a_rD^2/\nu)/dRe \,]\,(Re - Re_{cr}). \qquad (5.12)$$

This equation shows that the frequency in the saturation state varies linearly with ($Re - Re_{cr}$), with an offset given by the first term on the right hand side. From experiments, we can thus deduce the constant a_{io} (=a_i at Re_{cr}), and the combination of constants multiplying ($Re - Re_{cr}$). Among them, a_r is already known from (4.2), but to determine the other constants from this combination individually, we need to look at equation (5.10) again. If this equation is valid for the present problem, the following situation must occur. When the oscillations do occur in the flow, they must set in initially at a frequency equal to $a_i/2\pi$, which should then increase quadratically with the amplitude of oscillation (as shown qualitatively in figure 8a). As the amplitude saturates according to (5.9), so does the frequency according to

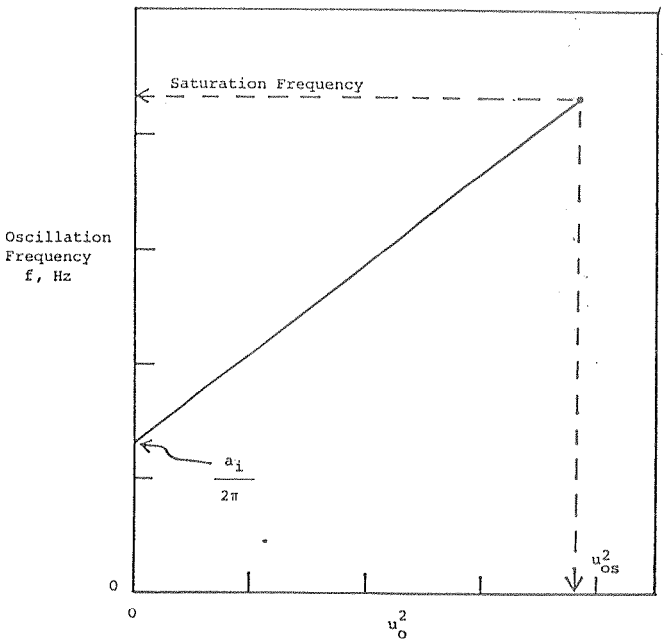

Figure 8a: Qualitative relationship between the frequency and the amplitude of oscillations. Oscillations commence at a frequency equal to $a_i/2\pi$.

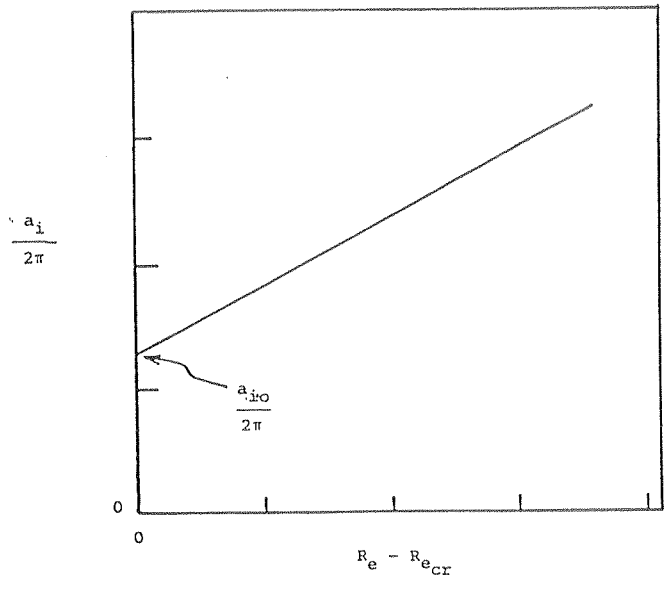

Figure 8 b: Qualitative dependence of the onset frequency $a_i/2\pi$, on the difference Reynolds number $R_e - R_{e_{cr}}$.

(5.12). Data similar to figure 8a, obtained at various Reynolds numbers, may now be plotted as in figure 8b to give a_{io} (the same as that obtained from equation (5.12)) as well as da_i/dRe. This now gives us the combination c_{ro}/c_{io}. But since c_{ro} is already known from (5.9), c_{io} can be calculated also. It should be noted that since c_{ro} is likely to be a function of x/D, c_{io} will have a similar dependence.

We now return to the experimental determination of the remaining constants.

6. The remaining constants

6.1. The relation between the vortex shedding frequency and the Reynolds number: As we mentioned in section 3, it is well known that the vortex shedding frequency varies linearly with the Reynolds number. We show this again here by plotting in figure 9 the combination fD^2/ν, known both as the Stokes number and the Roshko number, for the three aspect ratios mentioned above. It is interesting to note that the slopes are different in the three cases, the largest value corresponding to the largest aspect ratio. For the largest aspect ratio data, the best fit gives

$$fD^2/\nu = 5.46 + 0.21(Re - Re_{cr}), \qquad (6.1)$$

which is quite close to the relation obtained by Roshko, equation (3.1). Comparing this with equation (5.12), we get

$$a_{io}D^2/2\pi\nu = 5.46, \qquad (6.2)$$

and the combination

$$(1/2\pi)\,[\, d(a_iD^2/\nu)/dRe - (c_{io}/c_{ro})\, d(a_rD^2/\nu)/dRe \,] = 0.21. \qquad (6.3)$$

To determine all the constants explicitly, we follow the procedure outlined at the end of section 5. From the experimentally determined relation between the frequency and amplitude of oscillations (figures 10a and b), it is seen that the quadratic relation (5.10) is indeed valid. Furthermore, the slopes from figures 10a and 10b, corresponding to Reynolds numbers 30 and 62 respectively, are nearly equivalent; this condition is approximately satisfied over a range of $(Re - Re_{cr})$. Since the slope $d(fD^2/\nu)/du_o^2 = -c_iD^2/2\pi\nu$, and is approximately independent of Reynolds number, we are justified in replacing (5.11) by (5.12) by neglecting $d(c_iD^2/\nu)/dRe$.

The intercept in figures 10 gives the constant a_i appropriate to the measurement Reynolds number. From many such plots, we obtain figure 11 which shows how a_i varies with Reynolds number; data has been collected for both amplified and damped disturbances. It is seen that the dependence is linear to a first approximation in the positive neighborhood of $(Re - Re_{cr})$, as envisaged earlier. This approximation becomes invalid for values of $(Re - Re_{cr}) < -10$.

In figure 11, the intercept of $a_iD^2/2\pi\nu$ with the line $Re = Re_{cr}$ gives the constant a_{io} (the same as (6.2)) and the slope, taken in the positive neighborhood of $(Re - Re_{cr})$, gives the constant $(1/2\pi)$

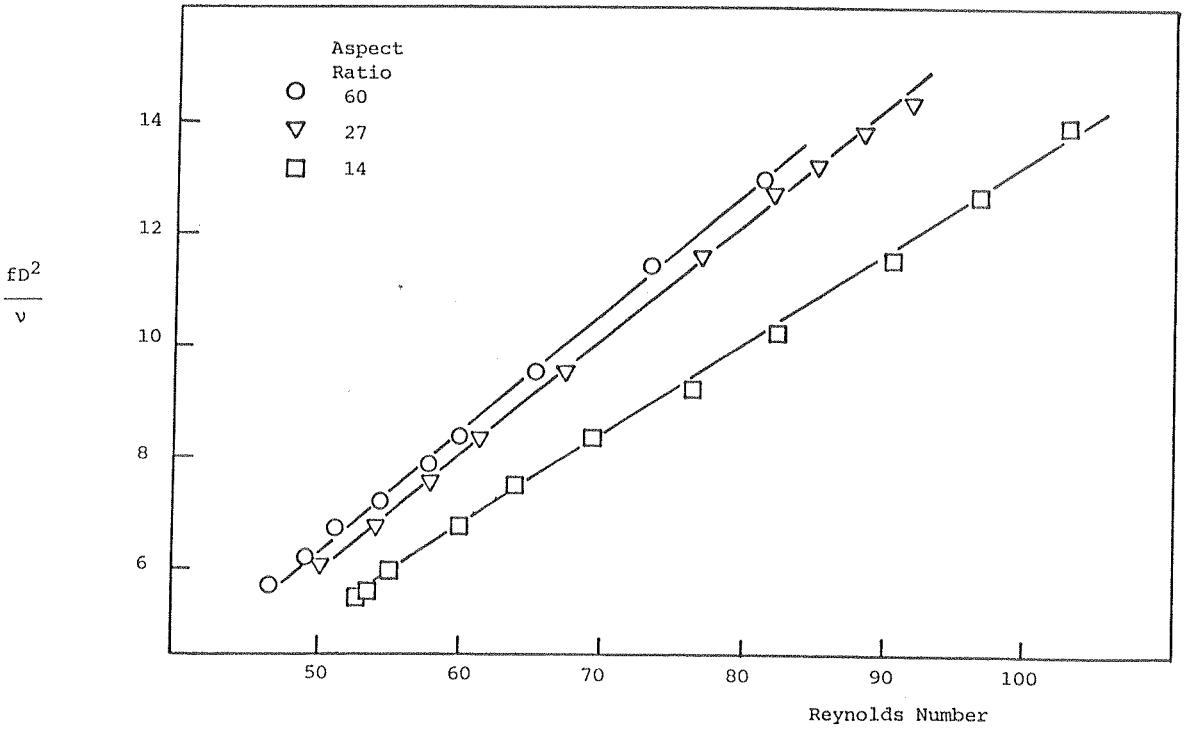

Figure 9: Vortex shedding frequency measured in the saturation state for three aspect ratios

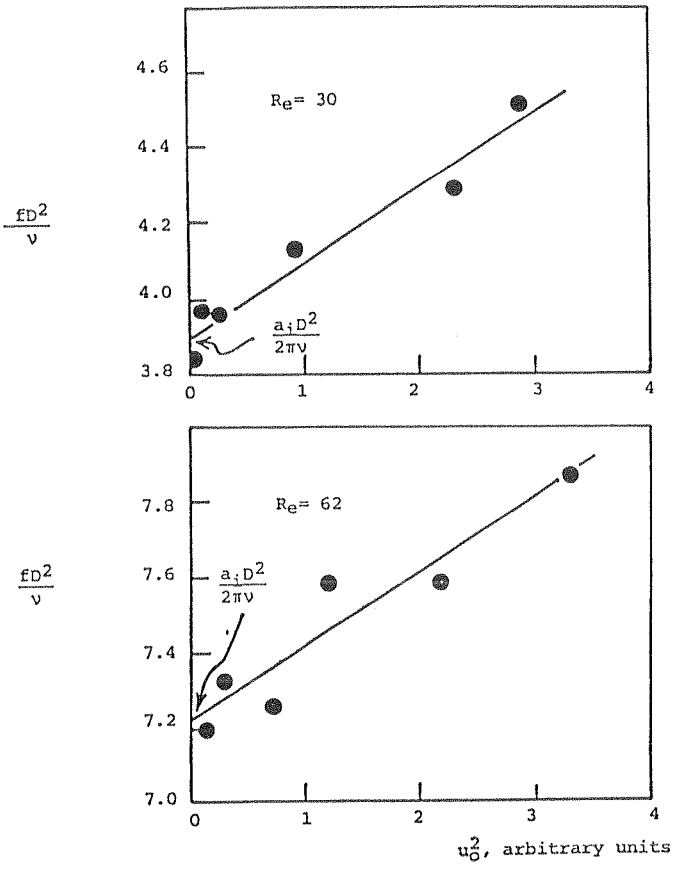

Figure 10: Relationship between frequency of oscillation and amplitude during decay at Re= 30 and during amplification at Re= 60. The intercept determines the onset frequency $a_i D^2/2\pi\nu$. L/D= 60.

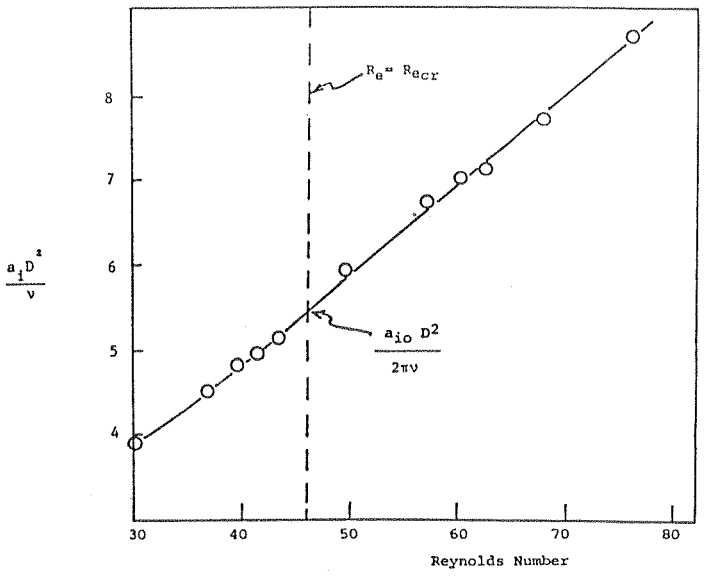

Figure 11: Dimensionless onset frequency as a function of the Reynolds number. L/D = 60.

$d(a_i D^2/\nu)/dRe$. From here, we have:

$$d(a_i D^2/\nu)/dRe = 0.7 \tag{6.4}$$

Putting them all in equation (6.3), we also have

$$c_{io} D^2/\nu = -202. \tag{6.5}$$

6.2 A further simplification: The number of constants required to specify the frequency and amplitude of oscillations in the periodic state are five according to the previous analysis. They are:

$$da_r/dRe,\ a_{io},\ da_i/dRe,\ c_{ro} \text{ and } c_{io}.$$

A rather simple observation reduces the number by one. This follows from a comparison of figures 6 and 9. The slopes $d(a_r D^2/\nu)/dRe$ and $d(fD^2/\nu)/dRe$ are nearly equal to each other at all aspect ratios even though the individual slopes do vary with the aspect ratio. To test this interesting conclusion further, we measured both the growth rates and the vortex shedding frequency for an aspect ratio of 5. Although these particular experiments were not very clean because of several operational difficulties associated with small aspect ratio cylinders - here, the reduction in the aspect ratio was achieved by bringing the artificial end plates closer - the conclusion regarding the slopes was borne out satisfactorily. It appears that the equality of the two slopes can be regarded as approximately true to within the experimental accuracy (see Table 2). The conclusion then is that

$$(1/2\pi)\, d(a_i D^2/\nu)/dRe = 1.05\, (c_{io}/2\pi c_{ro} + 1)\, d(a_r D^2/\nu)/dRe \tag{6.6}$$

which reduces the number of constants to four.

Table 2

Aspect Ratio	$d(fD^2/\nu)/dRe$	$d(a_r D^2/\nu)/dRe$
60	0.21	0.20
27	0.20	0.19
14	0.17	0.17
5	0.17	0.17

Here we summarize the experimentally determinated Landau constants for the large aspect ratio (L/D = 60).

$$a_r D^2/\nu = 0.20\ (Re - Re_{cr})\ . \qquad (6.7a)$$

$$a_i D^2/\nu = 34.3\ + 0.7\ (Re - Re_{cr}) \qquad (6.7b)$$

$$c_r D^2/\nu = 67 \qquad (6.7c)$$

$$c_i D^2/\nu = -202. \qquad (6.7d)$$

With the expectation that proper normalization should lead to numbers of the order unity, we renormalize c_r and c_i with the convective time scale D/U_o, reducing their magnitudes by the factor of Re. We obtain the constants:

$$c_r D^2/\nu) \ / \ Re = 1.2 \qquad (6.8a)$$

$$(c_i D^2/\nu) \ / \ Re = -3.5. \qquad (6.8b)$$

Realizing that the constants c_r and c_i govern the saturation or the vortex shedding state, and recalling that Karman's original analysis (see Lamb 1945, p224) predicted the structure of the wake from a completely inviscid model, it seems reasonable that these constants should be dictated by convective scales as opposed to viscous ones.

We should mention that there is some difficulty in obtaining accurate absolute numbers from figures 7 and 10, due to large spatial variation of the saturation amplitude in the near-wake region.We have chosen to obtain c_{ro} from the slope in figure 7 instead of c_{io} from the slope in figure 10. This choice was made because figure 7 is determined in the saturation state where the data tend to be more consistent. Independent of these difficulties it is clear that the ratio $c_{io}/c_{ro} = -3$ quite accurately from equation (6.3).

5. Is the wake absolutely unstable ?

5.1 The background: We have seen that many of the experimentally observed features of the vortex shedding process are locally in agreement with the Landau equation which is purely temporal in nature. But some of the Landau constants appear to vary from place to place in the wake, so that the problem may be thought of as being characterized by a combination of spatial and temporal features, the spatial aspects appearing only indirectly. It has been suggested (e.g., Monkewitz & Nguyen 1986, Strykowski 1986) that the wake instability giving rise to vortex shedding is an absolute type which is spatio-temporal in character. We introduce the concept of absolute instability briefly – for a more detailed discussion see Huerre & Monkewitz 1985 – and describe our measurements that may shed some light on the problem. The concepts of absolute and convective instability develop quite naturally from an analysis in which a disturbance packet containing all wavenumbers is introduced into an initially parallel shear flow field (basic state) and allowed to develop in both space and time. If the shear flow is unstable it will contain a group of amplified waves which travel at their group velocity, and the evolution of these amplified wavepackets determines the nature of the flow instability. A convective instability results if a wave packet introduced at a spatial position x_o and time t_o has a positive group velocity when amplified, so that it gets convected away with the flow, leaving the basic flow locally undisturbed for large times. If the amplified wave packet has zero group velocity, it grows locally and will eventually dominate the flow development. In a real system, non-linearities prevent the amplitude of the disturbance from becoming unbounded and a saturation amplitude is reached. In contrast to a convectively unstable flow where the amplified disturbance has contributions from all wavenumbers growing as they convect, an absolutely unstable flow is dominated by a pure frequency instability.

Now, it is well known that vortex shedding at low Reynolds numbers, unlike the case of the boundary layer instability, shows a pure frequency behavior (Kovasznay 1949, Roshko 1954). This was emphasized by Sreenivasan (1985), who showed that the pure frequency component could be seven or so orders of magnitude above the background noise. Prompted primarily by this observation, we have studied the vortex shedding process in the context of the absolute stability characteristics discussed above in qualitative terms. The conformity of this process with a purely temporal model (Landau equation) with spatially varying constants provides the additional incentive.

An absolutely unstable flow will be insensitive to the amplitude of the initial disturbance since this amplitude will only determine how long it takes for the disturbance to grow but will not affect the rate at which it grows or the saturation amplitude it eventually reaches. In contrast, a convectively unstable flow will be sensitive to initial disturbance amplitude. But, an absolutely unstable flow will show sensitivity to external geometric changes since it is dominated by a local instability. Hence an external device which locally alters the basic state (mean velocity profile) may profoundly affect the nature of instability. A convectively unstable flow is governed by a global instability, and hence altering the basic state locally will have little effect. Strykowski & Sreenivasan (1985) and Strykowski (1986) have discussed the dramatic effect that geometric changes can have on wake stability, showing that the placement of a second small cylinder in an appropriate position in the wake can severely alter and even completely suppress vortex shedding in a certain non-trivial Reynolds number range above the critical Reynolds number. In fact, Strykowski argues that the second cylinder suppresses shedding by altering the wake's stability from absolute to convective. A systematic study of the insensitivity of vortex shedding to the initial disturbance level has not been attempted, however. Below, we give some preliminary results addressing this question directly. We choose to alter the initial disturbance amplitude in two ways: external acoustic excitation and varying freestream turbulence level. We then study the effect on vortex shedding, in terms of the temporal growth rates, saturation amplitude, and the critical Reynolds number.

7.2 The insensitivity of the saturation amplitude to the excitation amplitude: The vortex shedding wake was acoustically excited using the experimental set-up detailed in figure 12. The acoustic excitation produced by the 10 cm. diameter speaker was monitored by a Bruel & Kjaer Type 1613 acoustic pressure meter (Type 4165 microphone) placed in the opposite test section wall. The excitation frequencies used were much lower than frequencies which would set up standing waves in the wind tunnel test section. The frequency of acoustic excitation was set at the natural shedding frequency for Re > Re_{cr} (= 43 for this particular flow). Below Re_{cr} the vortex shedding is artificially excited at the frequency which yields the largest wake response for a given acoustic excitation level (the least damped frequency). This Strouhal number St = fD/U_o for the least damped frequency was found to be very close to 0.1, the value suggested by Nishioka & Sato (1978). A hot wire placed at an x/D = 10 measured the x-component wake response of the velocity to the acoustic excitation. As discussed previously one would expect an absolutely unstable flow to yield a saturation amplitude which is independent of the initial disturbance amplitude. In figure 13, which shows the saturation amplitude vs acoustic excitation level, we see that this is indeed the case for Re > 46, the wake response being flat to excitation levels up to 25 dB above background noise levels. In sharp contrast is the wake response for Re < 40, which shows an approximately linear response to acoustic excitation level (see especially the Re = 40 case). This suggests that the flow over a circular cylinder for Reynolds number below critical is indeed convectively unstable. It should be noted that it was difficult to artificially excite vortex shedding below Re = 27 suggesting that the flow becomes completely stable at these low Reynolds numbers.

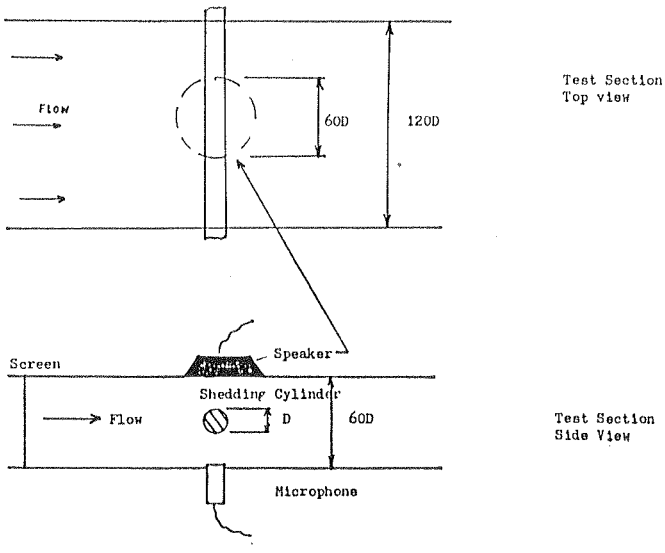

Figure 12: Schematic of apparatus for acoustic excitation work.

7.3. The insensitivity of temporal growth rates and the critical Reynolds number to the background noise level: This question was studied in the same facility used to measure growth and decay rates described in section 3. Freestream turbulence level was increased by placing additional screens approximately 100 diameters upstream of the shedding cylinder. The freestream turbulence level was varied from 0.03% to 0.19%. Temporal growth rates were determined as previously discussed. A hot wire placed in the wake at x/D = 10 measured the temporal growth of the x-component of velocity. The aspect ratio for this experiment was approximately 60. Figure 14 shows the temporal growth rates vs Reynolds number for three different freestream turbulence levels. Within experimental scatter we see that all data collapses onto a single line with slope da_r/dRe = 0.20, thus highlighting the insensitivity of temporal growth rates to freestream turbulence levels.

From the growth rate data, we have obtained the critical Reynolds numbers at different noise levels by determining where the least square fits to the growth rate data intersect the abscissa (corresponding to the zero growth rate condition); see figure 15. We note the insensitivity of critical Reynolds number as freestream turbulence level is varied and compare this to the well known sensitivity of Re_{cr} in a convectively unstable flow such as the boundary layer on a flat plate.

8. Summary

Writing again **u** as $u_o \exp(i\phi)$, noting that $u_o = \exp(a_r t)$, and, from (5.3) that $d\phi/dt = a_i$ for small amplitudes, we have:

$$\begin{bmatrix} \dot{u}_r \\ \dot{u}_i \end{bmatrix} = \begin{bmatrix} a_r & -a_i \\ a_i & a_r \end{bmatrix} \begin{bmatrix} u_r \\ u_i \end{bmatrix}$$

The square matrix in the above eqation gives the matrix A in equation (2.1). The eigenvalues of this matrix are easily shown to be $a_r \pm ia_i$, both known from measurement. From this, we can now determine how the eigenvalues journey in the complex plane as Reynolds number increases from below Re_{cr} to above Re_{cr}. This is done in figure 16. Clearly, the eigenvalues cross the imaginary axis at Re_{cr} (which by definition corresponds to $a_r = 0$). Also, the speed at which the real part of the eigevalues cross the imaginary axis is given by da_r/dRe which, by equation (4.2) is equal to $0.2\nu/D^2$.

We have thus shown that the onset of vortex shedding occurs strictly according to the Hopf bifurcation. We have also shown that, in a certain non-trivial neighborhood of the critical Reynolds number, the supercritical state is described by the Landau equation. This may at first appear surprising because intuition suggests that the problem must be spatial in character. One important finding of this work is that the spatial nature of the problem appears only in a secondary role, namely in the spatial dependence of some of the Landau constants. We have also shown that the growth rates, saturation amplitudes, and

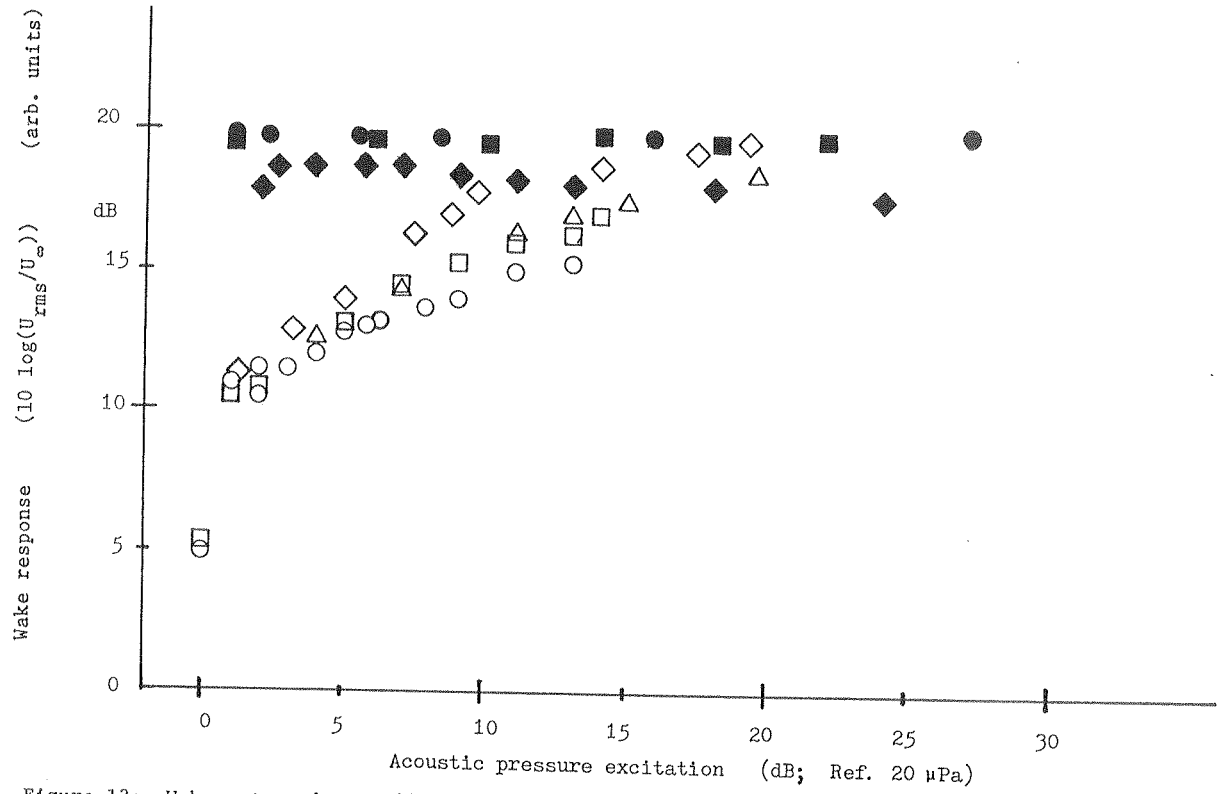

Figure 13: Wake saturation amplitude vs. external acoustic excitation; ○ Re = 27; □ Re = 30; △ Re = 36; ◆ Re = 46; ■ Re = 51; ● Re = 61; Aspect ratio = 60. Hot wire position, x/D = 10.

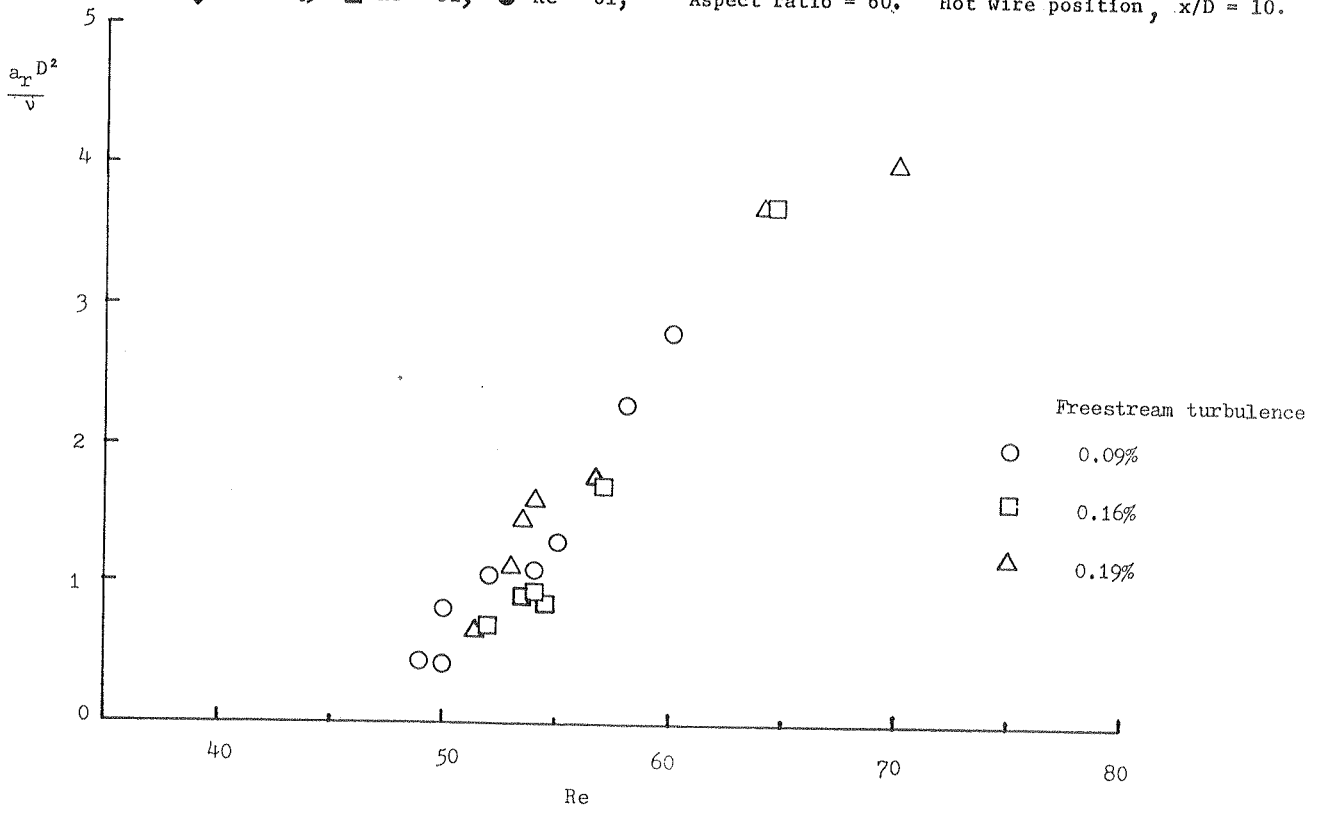

Figure 14 Growth rates at different freestream turbulence levels.

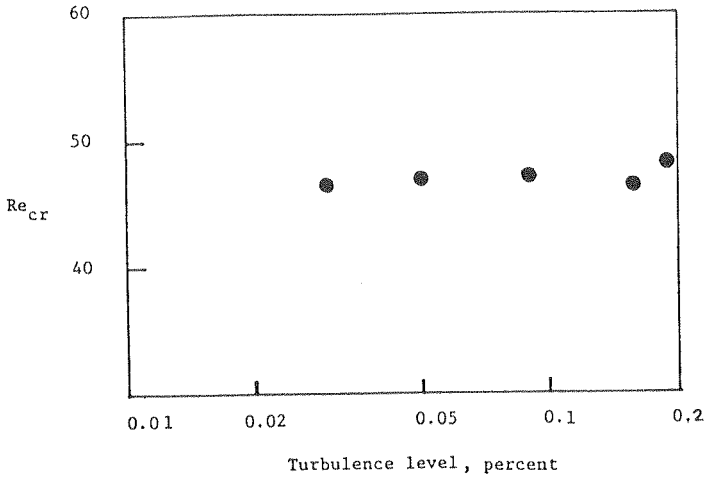

Figure 15: Critical Reynolds numbers as a function of freestream turbulence level.

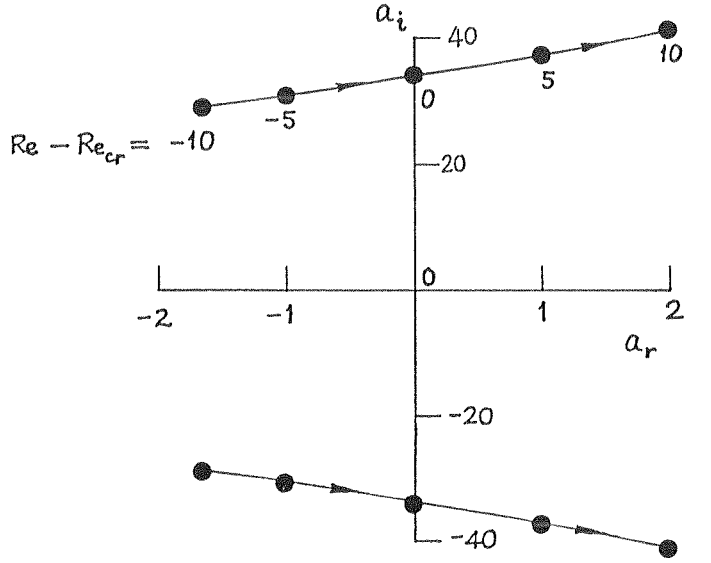

Figure 16: As the Reynolds number increases from below Re_{cr} to above Re_{cr}, the complex conjugate eigen values of the matrix A in (2.1) move from the left half of the complex plane to the right.

the critical Reynolds number associated with the vortex shedding process are robust against the background noise level. This is in contrast with many other familiar fluid flows such as constant-density cold jets and boundary layers, and in this sense the vortex shedding process in wakes shares some of the very important characteristics of dynamical systems. It is expected that most of these aspects will be discussed in greater detail in a forthcoming publication.

After this work was completed, we came across a paper (Mathis et al., 1984) and a report (Provansal et al., 1986) which independently make measurements similar to the ones reported here. We have not yet had the opportunity for a detailed comparative study of the two sets of measurements. This too is anticipated to occur in the near future.

HUERRE, P. and MONKEWITZ, P.A. 1985 *Absolute an convective instabilities in free shear layers*, J. Fluid Mech. **15** 151-168.

KOVASZNAY, L.S.G. 1949 *Hot-wire investigation of the wak behind cylinders at low Reynolds numbers*, Proc. Roy. Soc. Lond A **198**, 174-190.

LAMB, H. 1945 *Hydrodynamics*, Dover Publications 6th edition.

LANDAU, L.D. and LIFSHITZ, E.M. 1959 *Fluid Mechanics-Vo 6 Course of theoretical physics*, Pergamon Press London.

MATHIS, C., PROVANSAL, M. and BOYER, L. 1984 *Th Benard-Von Karman instability: an experimental study near th threshold*, J. de Phys. Lett. 45, L483-491.

MONKEWITZ, P. & NGUYEN, L.N. 1986 *Frequency selection jets and wakes*, submitted to J. Fluids and Structures.

NISHIOKA, M. and SATO, H. 1974 *Measurements of velocit distributions in the wake of a circular cylinder at low Reynold numbers*, J. Fluid Mech. 65, 97-112.

NISHIOKA, M. and SATO, H. 1978 *Mechanism of determinatio of the shedding frequency of vortices behind a cylinder at lo Reynolds numbers*, J. Fluid Mech. **89**, *49-60*.

PROVANSAL, M., MATHIS, C. and BOYER, L. 1986 *Benard-vo Karman instability: Transient and forced regimes*, submitted to Fluid Mech.

ROSHKO, A. 1954 *On the development of turbulent wakes fron vortex streets*, NACA Rep. 1191.

SREENIVASAN, K.R. 1985 *Transition and turbulence in flui flows and low-dimensional chaos*, in "Frontiers in Fluid Mechanics' (ed. Davis, S.H. and Lumley, J.L.) Springer-Verlag, 41-67.

STANSBY, P.K. 1974 *The effects of end plates on the bas pressure coefficient of a circular cylinder*, Aero. Journal 78, 36-37.

STRYKOWSKI, P.J. (1986) *The control of absolutely an convectively unstable flows*, Ph. D. thesis, Yale University.

STRYKOWSKI, P.J. and SREENIVASAN, K.R. 1985 *Th control of transitional flows*, AIAA Shear Flow Control Conferenc Boulder Colorado, March 12-14.